1521-0103/355/1/86–98$25.00
THE JOURNAL OF PHARMACOLOGY AND EXPERIMENTAL THERAPEUTICS

http://dx.doi.org/10.1124/jpet.115.224832
J Pharmacol Exp Ther 355:86–98, October 2015

Biodistribution and Efficacy of Targeted Pulmonary Delivery of a Protein Kinase C-δ Inhibitory Peptide: Impact on Indirect Lung Injury

Mark J. Mondrinos, Linda C. Knight, Paul A. Kennedy, Jichuan Wu, Matthew Kauffman, Sandy T. Baker, Marla R. Wolfson, and Laurie E. Kilpatrick

Center for Inflammation, Clinical and Translational Lung Research (M.J.M., P.A.K., J.W., M.K., S.T.B., M.R.W., L.E.K.), Department of Physiology (M.J.M., P.A.K., J.W., S.T.B., M.R.W., L.E.K.), Sol Sherry Thrombosis Research Center (M.J.M., L.C.K., L.E.K.), Departments of Pediatrics and Medicine (M.R.W.), and Department of Radiology (L.C.K.), Temple University School of Medicine, Philadelphia, Pennsylvania

Received April 1, 2015; accepted August 3, 2015

ABSTRACT

Sepsis and sepsis-induced lung injury remain a leading cause of death in intensive care units. We identified protein kinase C-δ (PKCδ) as a critical regulator of the acute inflammatory response and demonstrated that PKCδ inhibition was lung-protective in a rodent sepsis model, suggesting that targeting PKCδ is a potential strategy for preserving pulmonary function in the setting of indirect lung injury. In this study, whole-body organ biodistribution and pulmonary cellular distribution of a transactivator of transcription (TAT)–conjugated PKCδ inhibitory peptide (PKCδ-TAT) was determined following intratracheal (IT) delivery in control and septic [cecal ligation and puncture (CLP)] rats to ascertain the impact of disease pathology on biodistribution and efficacy. There was negligible lung uptake of radiolabeled peptide upon intravenous delivery [<1% initial dose (ID)], whereas IT administration resulted in lung retention of >65% ID with minimal uptake in liver or kidney (<2% ID). IT delivery of a fluorescent-tagged (tetramethylrhodamine-PKCδ-TAT) peptide demonstrated uniform spatial distribution and cellular uptake throughout the peripheral lung. IT delivery of PKCδ-TAT at the time of CLP surgery significantly reduced PKCδ activation (tyrosine phosphorylation, nuclear translocation and cleavage) and acute lung inflammation, resulting in improved lung function and gas exchange. Importantly, peptide efficacy was similar when delivered at 4 hours post-CLP, demonstrating therapeutic relevance. Conversely, spatial lung distribution and efficacy were significantly impaired at 8 hours post-CLP, which corresponded to marked histopathological progression of lung injury. These studies establish a functional connection between peptide spatial distribution, inflammatory histopathology in the lung, and efficacy of this anti-inflammatory peptide.

Introduction

Sepsis and associated multiple organ failure remain a leading cause of death in intensive care units (Stevenson et al., 2014). The lung is susceptible to systemic inflammation, leading to an acute lung injury. The action of circulating mediators, activated leukocytes, and pathogens induces pulmonary vascular inflammation and elevated neutrophil influx, causing indirect acute inflammatory lung injury (Perl et al., 2011), which can develop into acute respiratory distress syndrome (ARDS) (Matthay and Zemans, 2011; Ranieri et al., 2012). Despite improvements in clinical management, mortality rates above 40% persist (Villar et al., 2014), and there are no specific pharmacologic therapeutics for the treatment of ARDS (Iskander et al., 2013; Deutschman and Tracey, 2014). The systemic inflammatory response initiated during sepsis presents a myriad of proinflammatory mediators that activate multiple overlapping and redundant mechanisms. One potential approach in therapeutic design is to target common control signaling points which are activated by diverse signals (Gaestel et al., 2009; Cohen, 2009; Muller and Knapp, 2010).

Protein kinase C-δ (PKCδ) is activated by mediators involved in the septic response, including endotoxin, tumor necrosis factor, and interleukin-1β (Page et al., 2003; Kilpatrick et al., 2010; Mondrinos et al., 2013), functioning to integrate proinflammatory activities in pulmonary epithelial cells, endothelial cells, macrophages, and circulating leukocytes during acute lung inflammation (Mondrinos et al., 2013). Inflammatory pathologies such as ischemia-reperfusion (Chou et al., 2004) and endotoxin-induced lung injury (Chichger et al.,

This work was supported in part by the National Institutes of Health [Grants HL111552 to L.E.K. and 5T32-HL007777 to M.J.M.] and the Department of Defense/Office of Naval Research [Grants N00014-12-1-0597 and ONR N00014-12-1-0810 to M.R.W.].

L.E.K. is listed as an inventor on U.S. patent 8,470,766 entitled "Novel Protein Kinase C Therapy for the Treatment of Acute Lung Injury," which is assigned to Children's Hospital of Philadelphia and the University of Pennsylvania.

dx.doi.org/10.1124/jpet.115.224832.

ABBREVIATIONS: Aq5, aquaporin-5; ARDS, acute respiratory distress syndrome; CLP, cecal ligation and puncture; ID, initial dose; IT, intratracheal; MPO, myeloperoxidase; ^{99m}Tc, technetium radioisotope; PBS, phosphate-buffered saline; PKC, protein kinase C; pPKC, phosphorylated PKC; TAT, transactivator of transcription; TMR, 5,6-carboxytetramethylrhodamine.

2012) are attenuated in PKC$\delta^{-/-}$ mice. We have shown that selective PKCδ inhibition attenuates acute lung inflammation, reduces alveolar-capillary permeability and pulmonary edema, and preserves lung architecture in a rat model of sepsis-induced acute lung injury (Kilpatrick et al., 2011; Mondrinos et al., 2014). Therefore, targeting PKCδ is a potential strategy for the treatment of indirect acute inflammatory lung injury.

Although a proinflammatory role for PKCδ has been established, less is known about how PKCδ is activated during the systemic inflammatory response. PKCδ is regulated by phosphorylation patterns, subcellular translocation, and enzyme cleavage in a context-dependent manner (Kronfeld et al., 2000; Steinberg, 2004, 2008; Qvit and Mochly-Rosen, 2014). Two important tyrosine phosphorylation sites are PKCδ Tyr155, which is critical for nuclear translocation, and PKCδ Tyr311, which regulates enzyme cleavage and enhanced catalytic activity, alterations associated with proinflammatory signaling, and cytotoxic/apoptotic pathways (Humphries et al., 2008; Zhao et al., 2012). The phosphorylation patterns of pulmonary PKCδ during sepsis-induced acute lung injury are not known.

Intratracheal (IT) instillation of therapeutics is a commonly used delivery route in models of lung disease, as it produces a localized pulmonary effect (MacIntyre, 2001; Cheong et al., 2010). As a caveat, delivery of macromolecular therapeutics such as peptides to the lung interstitium and endothelium requires traversing of the pulmonary epithelial barrier, thereby necessitating the use of a "carrier" moiety. The trans-activator of transcription (TAT) peptide of human immunodeficiency virus-1 has cell-penetrating properties and the ability to deliver cargo to multiple organs (Schwarze et al., 1999). The protein transduction properties of this peptide have been exploited to facilitate intracellular delivery of a myriad of agents (Torchilin et al., 2001; Vives et al., 2003; Begley et al., 2004; Kleemann et al., 2005; Cai et al., 2006; Moschos et al., 2007; Nguyen et al., 2008; Qin et al., 2012; Bai et al., 2015).

In the current study, we examined whole-body regional biodistribution, global organ uptake, and spatial distribution on the cellular level within the lung parenchyma of a TAT-conjugated PKCδ inhibitory peptide (PKCδ-TAT) following IT delivery in control and septic rats. This well characterized inhibitor targets PKCδ-specific protein-protein interactions and modulates subcellular localization and activity of PKCδ (Chen et al., 2001; Qvit and Mochly-Rosen, 2014). This peptide exhibits low toxicity and is well tolerated in animal models at doses >1 mg/kg/day (Qi et al., 2008). Furthermore, in a phase I/II clinical trial to test safety and efficacy, no adverse events were reported following intracoronary injections of the PKCδ-TAT peptide in patients (up to 5 mg/patient) undergoing percutaneous coronary intervention (Bates et al., 2008; Churchill et al., 2008).

Systemic and cellular distribution of this or similar peptides in the lung following IT delivery has not been reported previously. Little is known about PKCδ activation in the lung in response to indirect pulmonary injury and the impact of the PKCδ-TAT inhibitor on PKCδ phosphorylation, translocation, and activation. Finally, there is a poor understanding of how pathologic progression of lung injury influences biodistribution and, consequently, efficacy. We sought to establish a functional connection between peptide spatial distribution in the lung and anti-inflammatory efficacy of this peptide inhibitor in the context of sepsis progression and development of indirect pulmonary injury.

Materials and Methods

PKCδ Inhibitory Peptide Synthesis. As previously described (Kilpatrick et al., 2011), PKCδ activity was selectively inhibited by a peptide antagonist (δV1.1 PKC-Tat peptide) that consists of a sequence derived from the first unique region (V1) of PKCδ (SFNSYELGSL: amino acids 8–17) coupled via an N-terminal Cys-Cys disulfide bond to a membrane permeant peptide sequence in the human immunodeficiency virus TAT protein (YGRKKRRQRRR: amino acids 47–57 of TAT) (Chen et al., 2001). The PKCδ-TAT peptide was also synthesized with a fluorescent tag (5,6-carboxytetramethylrhodamine [TMR]) at a noncritical site on the inhibitor portion of the peptide complex (Mimotopes, Melbourne, Australia). For radiolabeling studies, technetium radioisotope (^{99m}Tc) was attached to the PKCδ-TAT peptide utilizing hydrazine nicotinamide chemistry as described previously (Knight et al., 2007).

Animal Protocols. All animal handling and care adhered to National Institutes of Health standards and were approved by the Institutional Animal Care and Use Committee at Temple University School of Medicine. Male Sprague-Dawley rats (300–350 g; Charles River, Boston, MA) were used in all experiments. Rats were acclimated for at least 1 week in a climate-controlled facility and given free access to food and water.

Cecal Ligation and Puncture Model. Sepsis was induced by the cecal ligation and puncture (CLP) method as described previously (Rittirsch et al., 2009; Kilpatrick et al., 2011; Mondrinos et al., 2014). Sham controls underwent a laparotomy without cecal ligation or puncture. Following CLP or sham surgery, the abdominal incision was closed and the animals were orally intubated with a 16-gauge intravenous cannula. The animals were then maintained with mechanical ventilation (for short-term nonsurvival distribution experiments) or instilled with peptide or vehicle [phosphate-buffered saline (PBS)] and allowed to recover (for therapeutic experiments). For delayed delivery/treatment experiments, animals were orally intubated at either 4 or 8 hours following CLP or sham surgery and maintained with or without mechanical ventilation for distribution and therapeutic experiments, respectively. Postoperative pain was managed by injection of 2 mg/kg bupivacaine (Marcaine, Hospira Inc., Lake Forest, IL) at the incision site prior to surgery, then every 8–12 hours postoperatively until euthanasia. Normal saline solution (50 ml/kg) was injected subcutaneously in all groups for fluid resuscitation.

Biodistribution Studies. Animals were anesthetized with isoflurane, then orally intubated and ventilated with a tidal volume of 6 ml/kg (Rose et al., 2014; Sutherasan et al., 2014). The ventilation circuit was fit with a T-piece that allowed for direct insertion of a 23-gauge needle into the intubation cannula hub for intratracheal peptide instillation of between 50 and 500 μg/kg in sample volumes of between 200 and 600 μl. For intravenous delivery, the peptide was administered through a tail vein. All biodistribution experiments were carried out for 30 minutes following peptide instillation.

For ^{99m}Tc (radiolabel) studies, to analyze movement of radiolabeled peptide in real time, the instillation was performed with the animal lying supine on the detector face of a gamma camera. The camera (Maxicamera; Genera; Electric Medical Systems, Milwaukee, WI) was interfaced to a digital image collection system (NucLear Power; Scientific Imaging, Crested Butte, CO) and was fitted with a Low Energy All Purpose collimator. The energy discriminator was set for the 140-keV photopeak of ^{99m}Tc with a 10% window. Static images of 10-minute durations were collected in a 256×256 word mode matrix, beginning with labeled peptide (30–50 μCi of ^{99m}Tc) administration and sequentially without interruption during a 30-minute period of distribution. Following the 30-minute distribution period, the animal was euthanized and tissues, including lungs, heart, liver, kidneys,

spleen, skeletal muscle, fat, and blood, were harvested and weighed, then counted (Wizard 1480 counter; PerkinElmer, Waltham, MA) along with diluted standards of the administered dose. The raw counts for each organ were converted to the percentage of initial dose (ID) to quantify ^{99m}Tc-PKCδ-TAT biodistribution. For TMR (fluorescent tag) studies, peptide instillation and the biodistribution period were performed similarly, with the lungs cleared by vascular perfusion with heparinized saline solution, fixed and harvested (along with liver and kidney) as described later.

Efficacy Studies. Animals were randomized to receive PBS vehicle or the PKCδ-TAT inhibitory peptide at 50, 200, or 500 μg/kg in 400 μl of PBS. Sham-operated animals were also orally intubated and 400 μl of PBS delivered. For lung homogenate analysis [myeloperoxidase (MPO) activity assay as described later], lungs were cleared by vascular perfusion with heparinized saline solution, followed by dissection and snap freezing in liquid nitrogen.

Lung Fixation, Processing for Histology. Under continued anesthesia and mechanical ventilation, the thorax was opened and the lungs were fixed by vascular perfusion according to standard protocols (Fehrenbach et al., 1999) or by gravity fixation intratracheally as previously described (Mondrinos et al., 2014). Lung tissue samples were obtained from different locations in the left and right lung to assess the uniformity of delivered peptide distribution. Lung tissue was paraffin-embedded, cut into 5- to 10-μm sections, H&E stained, and stained with specific antibodies for immunohistochemistry as described previously (Mondrinos et al., 2014).

Lung Injury Scoring. Morphologic analysis of random fields ($n = 3$) from each section (minimum of $n = 9$ animals/group) was performed by a blinded investigator. Acute lung injury was scored based on the following parameters: 1) alveolar capillary congestion, 2) hemorrhage in the airspaces, 3) infiltration or aggregation of leukocytes in airspaces or vessel walls, and 4) thickness of the alveolar wall. The severity of each parameter was graded from 0 to 4 using the following convention: 0, no or little damage; 1, less than 25% damage; 2, 25–50% damage; 3, 50–75% damage; and 4, more than 75% damage. The average sum of all four lung injury parameters was compared among groups.

Immunohistochemistry. Antigen retrieval was achieved by boiling slides for approximately 10 minutes in citrate buffer, pH 6.0 (Mondrinos et al., 2014). Following antigen retrieval steps, slides were blocked with 3% bovine serum albumin for 1 hour. The sections were then incubated with rabbit polyclonal antibodies at dilutions of 1:40 for pPKCδ-311 (Cell Signaling Technology, Danvers, MA) and pPKCδ-155 (Santa Cruz Biotechnology, Dallas, TX) and 1:100 for pan-PKCδ (Santa Cruz Biotechnology) for 2–4 hours at room temperature. Secondary detection was performed using Alexa594-conjugated chicken anti-rabbit secondary antibody (Life Technologies, Grand Island, NY) diluted 1:500 with 4',6-diamidino-2-phenylindole included for nuclear counterstaining. For staining of CD68 (mouse monoclonal; Thermo Fisher Scientific, Waltham, MA), CD31 (rabbit polyclonal; Abcam, Cambridge, MA), and aquaporin-5 (goat polyclonal; Abcam) in lung sections from animals instilled with TMR-PKCδ-TAT to assess pulmonary cellular distribution, antigen retrieval had to be omitted due to loss of TMR fluorescence upon heating/boiling. As a consequence, primary antibody incubations were performed overnight in a humidified chamber at 4°C [1:50 for CD31, 1:50 for CD68, 1:50 for aquaporin-5 (Aq5)]. Secondary detection was performed with Alexa488-conjugated anti-goat and anti-mouse IgG (Life Technologies). Negative controls were processed by omitting the primary antibody in the protocol. Photomicrographs were taken using a fluorescence microscope equipped with a SPOT camera and image acquisition software (Spot Imaging Solutions).

MPO Activity Assay. Units of MPO enzymatic activity in lung tissue homogenates were measured as previously described (Salter et al., 2001), with modifications for use in a 96-well plate format. In brief, lung tissue was homogenized in freshly prepared lysis buffer (0.5% hexadecyltrimethyl ammonium bromide in 50 mM potassium phosphate buffer) at a ratio of 0.1 g of wet tissue weight per milliliter of lysis buffer. Homogenates were cleared by centrifugation at 13,362 $\times g$ for 15 minutes at 4°C and placed on ice. On a per-well basis, the reaction mixture contained 284 μl of 50 mM potassium phosphate buffer, 3 μl of H_2O_2, and 3 μl of 20 mg/ml o-dianisidine added to 10 μl of sample to initiate the reaction (300 μl total volume per well). Absorbance (460 nm) was measured over a 5-minute time course, and units of MPO activity were quantified using a standard curve.

Image Analysis. To establish a metric for PKCδ activation, a ratio of average pixel areas for PKCδ phosphorylated at the tyrosine 311 residue (pPKCδ_{311}) to total PKCδ was calculated. The pixel area for pan-PKCδ accounts for increased cellularity, i.e., numbers of PKCδ-expressing cells, thereby normalizing the measured pixel area of pPKCδ_{311} in relation to cellular infiltration. The number of pixels with fluorescence above the set threshold was then measured in ImageJ (National Institutes of Health, Bethesda, MD) using the area calculation feature. For normalization of TMR-PKCδ-TAT fluorescence in lung tissue sections, the measured pixel area of TMR fluorescence for sham-operated surgery at each time point (4, 8, and 24 hours post-CLP) was set equal to 1. For all image analyses, four animals per experimental group were analyzed, with at least two slides per animal and a minimum of 10 randomly positioned fields per slide, for a minimum of 80 images analyzed per experimental group.

PKCδ Translocation. PKCδ translocation to nuclear fractions was determined in lung tissue homogenates using a Subcellular Protein Fractionation Kit for Tissues (Thermo Fisher Scientific, Waltham, MA). In brief, 100 mg of lung tissue was homogenized in tissue lysis buffer containing protease inhibitors and the nuclear fraction isolated according to the manufacturer's instructions. Samples for Western blot analysis were prepared by mixing an aliquot of the nuclear extracts with 4$\times$ sample buffer and heating for 5 minutes at 95°C. Purity of nuclear fractions was routinely determined by probing fractions for cytoplasmic (lactate dehydrogenase) and nuclear (HDAC-2) markers.

Nuclear proteins (30 μg/lane) were separated on 4–12% SDS-PAGE gels and transferred to nitrocellulose membranes as described previously (Mondrinos et al., 2014). PKCδ nuclear translocation was determined by immunoblotting using a pan-PKCδ antibody (Santa Cruz Biotechnology). Translocation of PKCδ to the nucleus was quantitated by densitometry analysis of Western blots with ImageJ software version 1.46r (National Institutes of Health), and the values were expressed in arbitrary densitometry units.

PKCδ Cleavage. Whole-cell extracts were prepared from lung tissue for full-length and cleaved PKCδ detection as described previously (Kilpatrick et al., 2011). In brief, an aliquot (0.15 g) of frozen lung tissue was homogenized in 3 ml of buffer containing 10 mM Hepes (pH 7.4), 150 mM NaCl, 5 mM EDTA, 1 mM Na-orthovanadate, 20 μM 4-(2-aminoethyl)-benzenesulfonyl fluoride, 1% Triton X-100, 5 μg/ml leupeptin, and phosphatase inhibitor cocktail and protease inhibitor cocktail (Sigma-Aldrich, St. Louis, MO). Protein concentrations of the cell lysates were determined by the bicinchoninic acid protein assay kit, according to the manufacturer's instructions (Thermo Scientific, Rockford, IL). Proteins (30 μg/lane) were separated on 4–12% SDS-PAGE gels and transferred to nitrocellulose membranes. Full-length and cleaved PKCδ were determined by Western blotting using an antibody directed against the C terminus of PKCδ (sc-937; Santa Cruz Biotechnology). Equal protein loading was confirmed by reprobing membranes with a β-actin antibody. PKCδ cleavage was quantitated by densitometry analysis of Western blots as described earlier.

Lung Function. At 24 hours after sham or CLP surgery, rats were anesthetized, supported with 100% inspired oxygen, and arterial blood samples were obtained. PaO_2 and $PaCO_2$ were measured by a blood gas analyzer (ABL 835; Radiometer, Copenhagen, Denmark). Alveolar-arterial oxygen differences A-aDO_2 an important indicator of pulmonary gas exchange efficiency and intrapulmonary shunt, was calculated as A-aDO_2 (mm Hg) = $[PiO_2-(PaCO_2/0.8)]-PaO_2$.

Statistics. Results are expressed as means ± S.E.M. Data were analyzed by one-way analysis of variance for multiple comparisons, followed by Student's t test for individual comparisons. The

Tukey-Kramer multiple comparisons post-test was used to evaluate the significance between experimental groups if analysis of variance indicated a significant difference; differences were considered significant when $P < 0.05$, with additional degrees of significance assigned for $P < 0.01$ and $P < 0.001$.

Results

Organ Biodistribution of ^{99m}Tc-Tagged PKCδ-TAT Peptide. Organ biodistribution was determined by injecting ^{99m}Tc -PKCδ-TAT peptide inhibitor i.v. or IT at a dose of 500 μg/kg in a 400-μl delivery volume. Examination of whole-body distribution of ^{99m}Tc -PKCδ-TAT following i.v. (tail vein) delivery versus IT delivery revealed dramatic differences in whole-body distribution (Fig. 1A). There was no evidence of lung uptake in animals that received i.v. delivery; rather, the liver, kidneys, and bladder were clearly visible, as was a clear silhouette of the entire body, indicative of distribution and uptake in the peripheral tissues (Fig. 1A, left). By contrast, focal lung uptake and retention were observed in animals that received IT delivery, with no appreciable uptake visible in distant organs or the peripheral tissues (Fig. 1A, right).

Analysis of peptide uptake in organs 30 minutes post-injection revealed only 0.56 ± 0.06% ID in the lungs following tail vein injection of the ^{99m}Tc -PKCδ-TAT peptide compared with 68.45 ± 6.6% ID following IT delivery of the same dose/volume ($P < 0.001$; Fig. 1B). Peptide uptake in the liver increased from 1.96 ± 0.58% ID for IT to 10.8 ± 2.1% ID for i.v. ($P = 0.056$). Peptide uptake was also significantly increased following i.v. administration as compared with IT delivery for kidney (1.4 ± 0.55% ID for IT to 12.7 ± 0.8% ID for i.v.; $P < 0.01$) and skeletal muscle (3.5 ± 0.85% ID for IT to 7.9 ± 0.9% ID for i.v.; $P < 0.05$). The only organ/tissue other than the lungs with higher % ID upon IT versus i.v. delivery was the trachea ($P < 0.05$; Fig. 1B). At 30 minutes after ^{99m}Tc -PKCδ-TAT administration, there was a nonsignificant increase in the amount of peptide present in the blood compartment from 4.9 ± 4.1% ID for IT to 7.6 ± 1.2% ID for i.v. delivery (Fig. 1B). Negligible amounts (<1% ID) of peptide were recovered from the heart and spleen in both cases (data not shown).

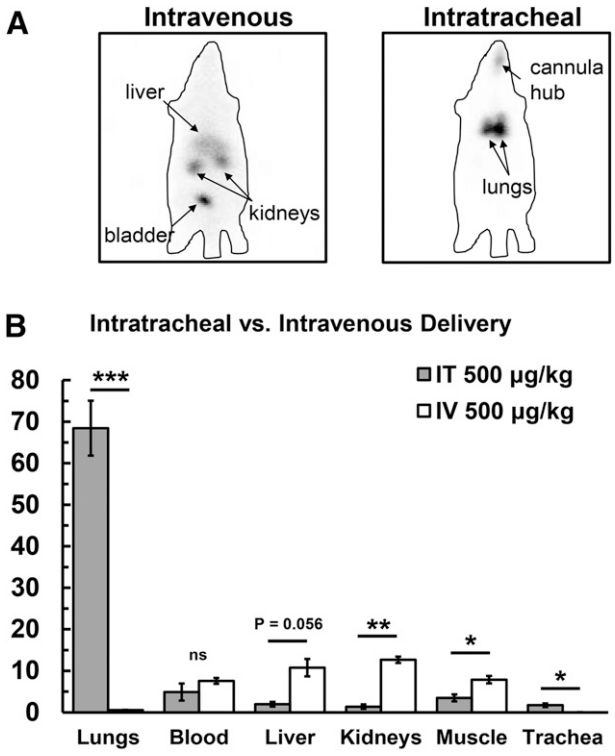

Fig. 1. Comparison of global ^{99m}Tc-PKCδ-TAT biodistribution following i.v. (tail vein) versus IT delivery of 500 μg/kg in 400 μl. (A) Gamma camera images; ^{99m}Tc signal is seen as black in panels. Liver, kidneys, and bladder are labeled in the intravenous panel. The lungs and signal from the endotracheal cannula hub are labeled in the intratracheal panel. Approximate outlines of the rat bodies are shown as a lined perimeter. (B) Percentage of ID for lung, blood, liver, kidney, skeletal muscle, and trachea for IT delivery (gray bars) and i.v. delivery (white bars). Data are expressed as means ± S.E.M. (n = 4 rats/group). *$P < 0.05$; **$P < 0.01$; ***$P < 0.001$. ns, not significant.

Comparing the total uptake for IT versus i.v. delivery showed that IT delivery facilitates greater than 100-fold enhancement in lung-targeting specificity while concomitantly reducing the total peptide present in the blood by approximately 35% and that taken up in the liver and kidneys by greater than 80% (Table 1). Comparing total organ uptake in relation to lung uptake for IT versus i.v. delivery showed that, following IT delivery, the blood contains approximately 7% of the total peptide present in the lung, whereas liver, kidney, and skeletal muscle all contain less than 5% of the peptide measured in the lung (Table 1). By contrast, i.v. delivery results in a greater than 10-fold increase relative to the amount of peptide in the lung for blood, liver, kidneys, and skeletal muscle (Table 1).

Effect of Volume/Dose on Lung Retention. To establish an optimal volume for delivery of the peptide at doses between 50 and 500 μg/kg, IT delivery of ^{99m}Tc-PKCδ-TAT was tested in volumes of 200, 400, and 600 μl, volumes well tolerated by rats of this size (Driscoll et al., 2000). The percentage of ID delivered was used to assess lung retention (Fig. 2A). At a dose of 50 μg/kg, there were no significant differences in organ distribution for all volumes tested. At the higher peptide concentration (500 μg/kg), lung retention was similar at the 400- and 600-μl volumes but was significantly reduced when the peptide was administered in the smaller volume (200 μl) (Fig. 2A; $P < 0.05$). Greater leakage from the lung observed for 500 μg/kg in 200 μl was reflected in elevated blood levels (Fig. 2B; $P < 0.05$) and increased uptake in the liver (Fig. 2C; $P < 0.05$) relative to 50 μg/kg in 200 μl. At 500 μg/kg, peptide levels in the blood and liver uptake were elevated for a 200-μl delivery volume compared with both 400 and 600 μl (Fig. 2, B and C; $P < 0.05$), whereas the increase in kidney uptake at 200 μl was only significant

TABLE 1

Organ-targeting specificity for IT versus i.v. delivery of ^{99m}Tc-PKCδ-TAT

The IT-to-i.v. ratio equals %ID IT/%ID i.v. for each organ. The organ-to-lung ratio equals %ID organ/%ID lung for IT and i.v. Data are calculated from the mean values of %ID data shown in Fig. 1.

Organ	IT-to-IV Ratio	Organ-to-Lung Ratio	
		IT	i.v.
Lungs	123	1	1
Blood	0.65	0.07	13.5
Liver	0.18	0.03	19.2
Kidneys	0.11	0.02	22.6
Skeletal muscle	0.44	0.05	14.1

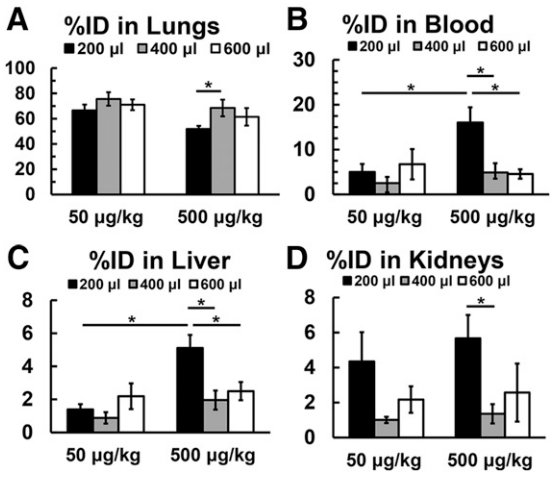

Fig. 2. Percentage of ID of ^{99m}Tc-PKCδ-TAT in the lungs (A), blood (B), liver (C), and kidneys (D) of normal rats (see *Materials and Methods*) at 30 minutes following IT delivery of 50 or 500 μg/kg in volumes of 200(black bars), 400(gray bars), and 600 μl (white bars). Data are expressed as means ± S.E.M. (n = 4 rats/group). *$P < 0.05$; **$P < 0.01$, with bars indicating individual comparisons.

compared with 400 μl (Fig. 2D; $P < 0.05$). Over the range of 50–500 μg/kg, a 400-μl delivery volume facilitated the greatest lung retention and lowest uptake in other organs.

^{99m}Tc-PKCδ-TAT Pulmonary Lobe Distribution Trends. To examine the distribution of ^{99m}Tc-PKCδ-TAT across the five pulmonary lobes, the ^{99m}Tc content was determined in each lobe separately, allowing for calculation of the total lung count percentages for each lobe (Table 2). Only the accessory lobe (the most inferior of the right lung lobes) had significantly different total count percentages for 50 versus 500 μg/kg delivered in 400 μl.

Intratracheal Delivery of PKCδ-TAT Attenuates Sepsis-Induced Lung Inflammation. We next assessed the anti-inflammatory effects of the PKCδ-TAT peptide over the concentration range of 50–500 μg/kg. Intra-abdominal sepsis produces systemic inflammation and influx of neutrophils into the lung, a hallmark of clinical ARDS (Abraham, 2003; Reutershan and Ley, 2004). The anti-inflammatory effects of the PKCδ-TAT inhibitory peptide were assessed by determining MPO activity in lung homogenates from unoperated (normal), sham surgery with IT instillation of 400 μl of PBS vehicle, and CLP-operated rats who received IT delivery of PBS vehicle or PKCδ-TAT at doses of 50, 200, and 500 μg/kg in 400 μl at the time of surgery (Table 3). At 24 hours postsurgery, sham surgery induced a detectable low-grade inflammatory response in the lung, as evidenced by a small but significant increase in lung MPO compared with unoperated rats ($P < 0.05$). CLP surgery induced a significant inflammatory response in the lung, as evidenced by a greater than 3-fold increase in lung tissue MPO activity relative to sham surgery ($P < 0.001$). All three doses of PKCδ-TAT significantly reduced CLP-induced lung MPO activity ($P < 0.01$ vs. CLP + PBS for all three doses), but the 200-μg/kg dose optimally inhibited sepsis-induced elevation of lung MPO activity ($P < 0.05$ vs. 500 μg/kg). Thus, the PKCδ-TAT peptide inhibitor was effective in attenuating sepsis-induced pulmonary inflammation over the concentration range used in the biodistribution studies.

Pulmonary Cellular Distribution of TMR-PKCδ-TAT. The ^{99m}Tc-PKCδ-TAT studies demonstrated significant lung retention of this peptide with IT delivery; however, this method does not permit resolution of spatial variations, e.g., proximal versus distal lung distribution. A fluorescent-tagged version of the peptide (TMR-PKCδ-TAT) was used to visualize the spatial distribution of the peptide in the lung following IT delivery (Fig. 3). TMR-PKCδ-TAT fluorescence in lung tissue sections revealed widespread and relatively uniform peptide distribution in the peripheral lung at 30 minutes postdelivery (Fig. 3A). By contrast, we did not detect significant TMR-PKCδ-TAT fluorescence in the liver (Fig. 3B) and kidney (not shown).

To identify peptide uptake in specific cell types, lung sections were stained with antibodies against CD68 (pan-macrophage marker; Fig. 3C), CD31 (endothelial marker; Fig. 3, D and E), and Aq5 (type I alveolar epithelial cell marker; Fig. 3F). Covisualization of TMR-PKCδ-TAT and CD68 revealed high levels of peptide uptake in pulmonary macrophages (Fig. 3C), with >85% of CD68-positive cells displaying TMR-PKCδ-TAT colocalization. Covisualization of CD31 and TMR-PKCδ-TAT revealed robust uptake throughout the endothelium in the peripheral lung (Fig. 3D). At a higher magnification, CD31-positive endothelial cells in the alveolar walls display TMR-PKCδ-TAT–rich cytoplasm (Fig. 3D, inset), with the majority of CD31-positive cells colocalizing TMR fluorescence (Fig. 3E). Covisualization of Aq5 and TMR-PKCδ-TAT revealed peptide uptake in alveolar type I cells (arrows in Fig. 3F); however, there is a substantial area of Aq5 staining without colocalized TMR fluorescence (Fig. 3F).

Intratracheal Delivery of PKCδ-TAT Reduces Sepsis-Induced Activation of PKCδ in Lung Tissue. In addition to cofactor regulation (i.e., diacylglycerol), PKCδ activity is also regulated by phosphorylation state, subcellular translocation, and cleavage (Steinberg, 2004, 2008). To establish a baseline assessment of PKCδ expression in the lungs of sham and CLP-operated animals, sections were stained with a pan-PKCδ antibody, and ubiquitous expression of PKCδ was observed throughout the lung parenchyma and in the cellular infiltrates induced by sepsis (Fig. 4A, top panels). PKCδ activation was first assessed by staining for pPKCδ$_{311}$, an

TABLE 2
Distribution of ^{99m}Tc-PKCδ-TAT in pulmonary lobes following IT administration
Data are the percentage of total lung counts of ^{99m}Tc-PKCδ-TAT in pulmonary lobes and are expressed as means ± S.E.M. (n = 4 rats/group).

	Percentage of Total Lung Counts				
PKCδ-TAT Dose	Left Lung	Cranial Lobe	Median Lobe	Caudal Lobe	Accessory Lobe
50 μg/kg	30.4 ± 5.3	5.9 ± 2.5	14.8 ± 2.9	39.7 ± 3.0	9.2 ± 1.1
500 μg/kg	30.0 ± 5.5	6.8 ± 3.8	14.4 ± 3.9	46.1 ± 6.3	2.7 ± 0.5*

*$P < 0.05$.

TABLE 3

PKCδ inhibition attenuates pulmonary MPO activity in sepsis

MPO activity is shown for unoperated rats (normal), sham surgery with IT instillation of 400 μl of PBS vehicle (sham), CLP surgery with IT instillation of 400 μl PBS vehicle (CLP + vehicle), and CLP surgery with IT instillation of 50, 200, and 500 μg/kg as indicated at the time of surgery. Tissue was harvested at 24 hours postsurgery. Data are expressed as means ± S.E.M. (n = 4 rats/group).

Conditions	Myeloperoxidase Activity
	units/g tissue
Normal	14.2 ± 3.2
Sham	25.5 ± 10.5*
CLP + vehicle (PBS)	82.7 ± 13.1***
CLP + 50 μg PKCδ-TAT/kg	55.9 ± 9.3**
CLP + 200 μg PKCδ-TAT/kg	46.5 ± 9.5**
CLP + 500 μg PKCδ-TAT/kg	62.5 ± 9.7**

*$P < 0.05$ versus normal; **$P < 0.01$ versus CLP + vehicle; ***$P < 0.001$ versus sham.

activation site shown to be phosphorylated during inflammation and toxin-induced tissue injuries (Pabla et al., 2011; Wong et al., 2011) (Fig. 4A, bottom panels), with a known role in enzymatic cleavage (Steinberg, 2004, 2008). Low levels of $pPKC\delta_{311}$ staining were observed in sham-operated lungs 24 hours postsurgery (ratio = 0.02; Fig. 4B). In contrast, 24 hours post-CLP, there was a significant increase in PKCδ phosphorylation at tyrosine 311, approximately 10-fold over sham (ratio = 0.18, $P < 0.01$; Fig. 4B), with intense staining observed throughout the alveolar walls. IT delivery of 200 μg/kg PKCδ-TAT significantly reduced sepsis-induced PKCδ phosphorylation by 50% (ratio = 0.09, $P < 0.05$; Fig. 4B), with marked reduction in alveolar wall cell staining.

Coimmunostaining for PKCδ phosphorylation at tyrosine 155 ($pPKC\delta_{155}$) with CD68 or rat endothelial cell antigen-1 allowed for assessment of PKCδ activation status in monocytes/macrophages and endothelial cells, respectively (Fig. 5). Sepsis (CLP) induced robust phosphorylation of PKCδ at tyrosine 155 (Fig. 5, C and D), whereas virtually no activation was observed in the lungs of sham-operated animals (Fig. 5, A and B). At the cellular level, some costaining of $pPKC\delta_{155}$ was observed in CD68-positive cells, indicating low levels of PKCδ activation in cells of the monocyte/macrophage lineage; however, most CD68-positive cells did not stain for $pPKC\delta_{155}$ (Fig. 5C). By contrast, the majority of endothelial cells expressing rat endothelial cell antigen-1 also stained intensely for $pPKC\delta_{155}$ (Fig. 5D). Similar to the pattern of inhibition observed for phosphorylation of tyrosine 311, IT delivery of PKCδ-TAT strongly inhibited tyrosine 155 phosphorylation (Fig. 5, E and F).

To further assess the inhibitory action of PKCδ-TAT, we assessed nuclear translocation and enzymatic cleavage of PKCδ in lung tissue homogenates. Nuclear translocation has been shown to be required for cytotoxic or proapoptotic function (Humphries et al., 2008; Pabla et al., 2011). To examine the impact of sepsis-induced inflammation on pulmonary PKCδ nuclear translocation, subcellular fractionation studies were carried out 24 hours after sham or CLP surgery. Little PKCδ was present in the nuclear fractions of

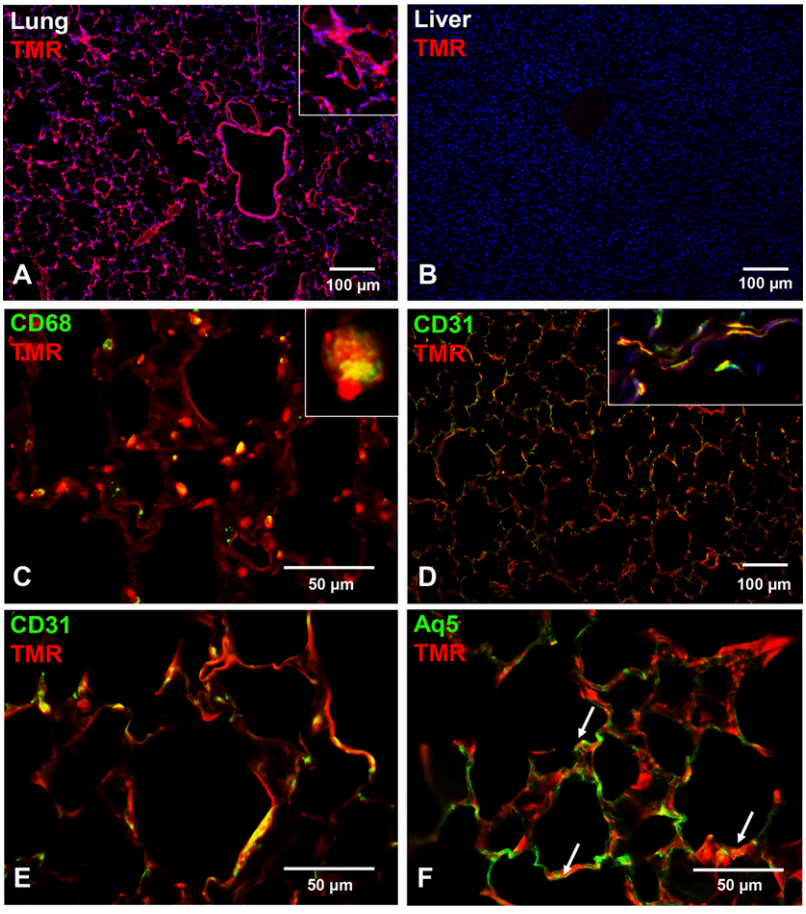

Fig. 3. Spatial and cell lineage–specific uptake of TMR-PKCδ-TAT in the lungs of normal (unoperated) animals 30 minutes following IT delivery of 400 μl of 200 μg/kg TMR-PKCδ-TAT. (A) Visualization of TMR-PKCδ-TAT uptake (red/orange fluorescence) throughout the airways, vasculature, and peripheral parenchyma/stroma; 4',6-diamidino-2-phenylindole (blue) nuclear counterstaining; scale bar = 100 μm; original magnification = 100×. (Inset) Cropped, enlarged view of area depicting TMR fluorescence in interstitial regions of the distal parenchyma. (B) Absence of TMR-PKCδ-TAT uptake (no detectable red/orange fluorescence) in a liver section from the same animal; 4',6-diamidino-2-phenylindole (blue) nuclear counterstaining; scale bar = 100 μm; original magnification = 100×. (C–F) Covisualization of cell lineage markers (green) with TMR-PKCδ-TAT (red/orange) in lung tissue sections. Yellow pixels indicate spatial colocalization, e.g., peptide uptake in cells expressing the labeled marker. (C) Covisualization of CD68 immunostaining TMR-PKCδ-TAT uptake to detect peptide uptake in macrophages; scale bar = 50 μm; original magnification = 400×. (Inset) Cropped and enlarged view of spatial colocalization of TMR and CD68 in a single macrophage. (D) CD31 immunostaining covisualized with TMR-PKCδ-TAT to detect peptide uptake in endothelial cells; scale bar = 100 μm; original magnification = 100×. (Inset) Cropped image from a separate field of view illustrating peptide uptake in endothelial cells of the alveolar walls; original magnification = 400×. (E) Higher magnification of CD31 immunostaining and TMR-PKCδ-TAT colocalization; scale bar = 50 μm; original magnification = 400×. (F) Aq5 immunostaining covisualized with TMR-PKCδ-TAT uptake to detect uptake in type I alveolar epithelial cells (yellow color, indicated by arrows); scale bar = 50 μm; original magnification = 400×.

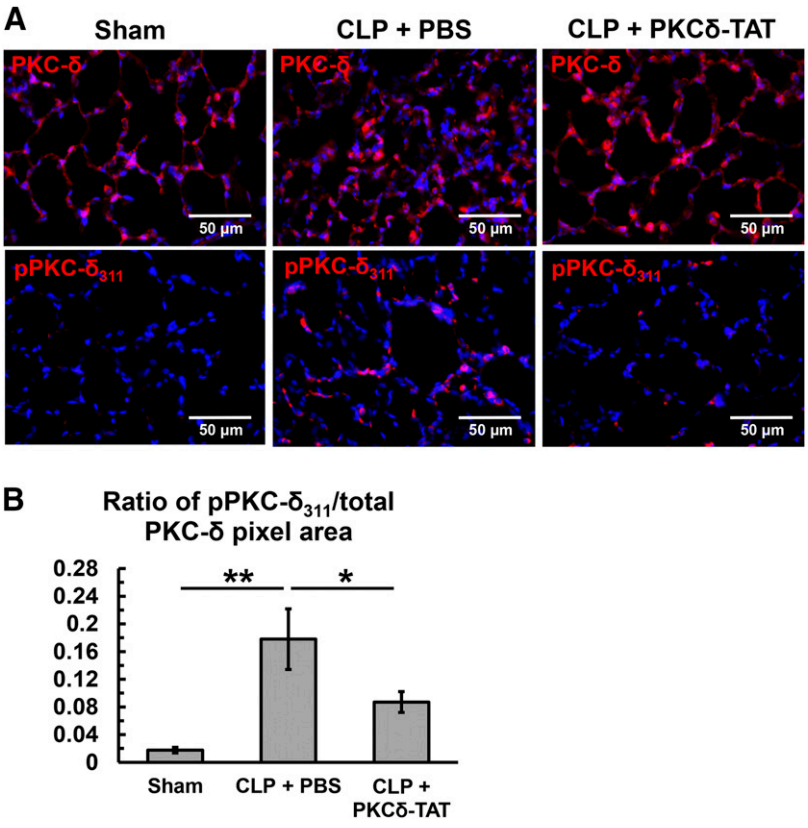

Fig. 4. Immunohistochemical analysis of PKCδ phosphorylation at tyrosine 311 in lung tissue sections at 24 hours postsurgery of sham-operated (Sham) animals (received 400 μl of PBS delivered IT) and CLP-operated animals that received 200 μg/kg PKCδ-TAT in 400 μl IT (CLP + PKCδ-TAT) or a similar volume of PBS vehicle only (CLP + PBS) immediately following surgery, as described in *Materials and Methods*. Original magnification = 400× and scale bars = 50 μm in all images. (A) Immunohistochemical detection of PKCδ and pPKCδ_{311} in lung tissue sections of sham operation (left column of panels), CLP with IT delivery of 400 μl of PBS vehicle (middle column of panels), and CLP with IT delivery of 200 μg/kg PKCδ-TAT in 400 μl (right column of panels). Positive signal for PKCδ (top row in A) and pPKCδ_{311} (bottom row in A) is seen as red fluorescence. 4',6-Diamidino-2-phenylindole was used for nuclear counterstaining (blue). (B) Ratio of pPKCδ_{311}-stained pixels to pan/total PKCδ–stained pixels to represent activation while accounting for increased cellularity and potential changes in baseline PKCδ expression; n = 4 animals per group, data were expressed as the mean ± S.E.M. prior to calculating the ratio; data are shown and statistically analyzed based on a calculated average ratio for each animal; $^*P < 0.05$; $^{**}P < 0.01$.

sham-operated lungs (Fig. 6A). In contrast, 24 hours post-CLP surgery, nuclear levels of PKCδ were significantly increased. IT delivery of PKCδ-TAT significantly reduced sepsis-induced nuclear PKCδ translocation in the lung by greater than 50% (Fig. 6A; $P < 0.05$).

During inflammation, caspase-mediated cleavage of PKCδ may contribute to activity by removing the regulatory domain from the kinase domain (Ghayur et al., 1996; Pabla et al., 2011). As nuclear translocation is required for cleavage of PKCδ (DeVries-Seimon et al., 2007; Humphries et al., 2008), we next examined the effect of sepsis on PKCδ cleavage in lung tissue. Twenty-four hours post-CLP surgery, sepsis induced significant cleavage of PKCδ in lung tissue as compared with rats that underwent sham surgery alone (Fig. 6B). IT delivery of 200 μg/kg PKCδ-TAT significantly reduced sepsis-induced PKCδ cleavage in the lung by greater than 60% (Fig. 6B; $P < 0.05$).

Intratracheal Delivery of PKCδ-TAT Improves Sepsis-Induced Decrease in Pulmonary Gas Exchange. Significant impairment of lung function was observed in septic animals who received IT PBS as compared with sham-operated animals, as evidenced by a significant increase in the alveolar to arterial oxygen pressure gradient (A-aDO_2) 24 hours post-CLP surgery (Fig. 7A). Sepsis-induced impairment of gas exchange and arterial oxygenation associated with increased intrapulmonary shunt was significantly reduced by IT delivery of PKCδ-TAT at the time of CLP surgery (Fig. 7A), demonstrating that attenuation of acute lung inflammation by this peptide is associated with improved pulmonary function. Preservation of pulmonary gas exchange corresponds to significant attenuation of early sepsis-induced histologic indirect lung injury at the 24 hours postsurgery time point (Fig. 7B). IT delivery of PKCδ-TAT significantly reduced sepsis-induced inflammatory infiltrate, preserved alveolar architecture and wall thickness, and reduced capillary congestion and hemorrhage (Fig. 7B, bottom panels), as evidenced by an approximately 50% reduction of scored values for histologic lung injury parameters (Fig. 7B; $P < 0.001$ for CLP + PKCδ-TAT vs. CLP + PBS).

Sepsis Progression Does Not Significantly Alter Whole-Body ^{99m}Tc-PKCδ-TAT Biodistribution. Little is known about the consequences of sepsis-induced lung inflammation and tissue damage in the biodistribution of PKCδ-TAT or similar peptides following IT administration. To address the effect of sepsis progression, 500 μg/kg ^{99m}Tc-PKCδ-TAT was delivered IT at 24 hours following sham or CLP surgery, when there is significant lung inflammation and tissue damage in this rat model (Kilpatrick et al., 2011; Mondrinos et al., 2014). Gamma camera imaging did not show any gross qualitative difference in the distribution of the peptide between sham- and CLP-operated animals (Fig. 8). Quantification of ^{99m}Tc-PKCδ-TAT counts in individual organs revealed similar relative distribution trends following sham and CLP surgery, with no significant differences compared with normal animals in organ-to-lung ratios of total peptide uptake in blood, liver, and kidney (Table 4).

Sepsis-Induced Pathologic Progression Disrupts Pulmonary Spatial Distribution. While there were no significant differences in lung distribution of ^{99m}Tc-PKCδ-TAT between sham- and CLP-operated animals at 24 hours postsurgery, we hypothesized that spatial distribution, e.g., uniformity of penetration into the alveoli, may be altered by sepsis progression. TMR-PKCδ-TAT fluorescence was quantified in lung tissue sections following IT delivery in sham- and

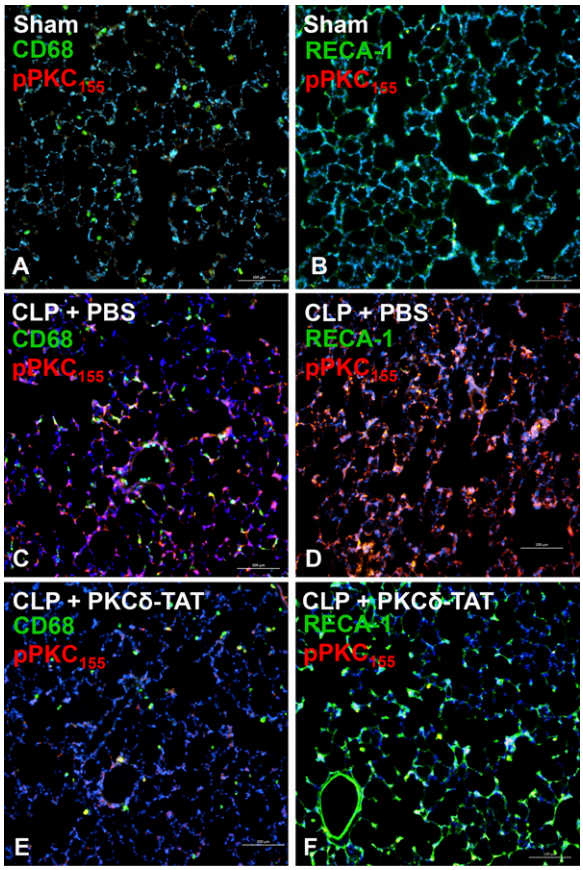

Fig. 5. Immunohistochemical analysis of $pPKC\delta_{155}$ in lung tissue sections at 24 hours postsurgery of sham-operated (Sham) (A and B) animals (received 400 μl of PBS delivered IT) and CLP-operated animals that received 200 μg/kg PKCδ-TAT in 400 μl IT (CLP + PKCδ-TAT) (E and F) or a similar volume of PBS vehicle only (CLP + PBS) (C and D) immediately following surgery, as described in *Materials and Methods*. All scale bars = 100 μm. (A, C, and E) Immunohistochemical detection of PKCδ phosphorylation at tyrosine 155 in pulmonary monocytes/macrophages. Double staining for CD68 (green) and $pPKC\delta_{155}$ (red); yellow/orange indicates colocalization. (B, D, and F) Immunohistochemical detection of PKCδ phosphorylation at tyrosine 155 in pulmonary endothelial cells. Double staining for rat endothelial cell antigen-1 (RECA-1; green) and $pPKC\delta_{155}$ (red); yellow/orange indicates colocalization.

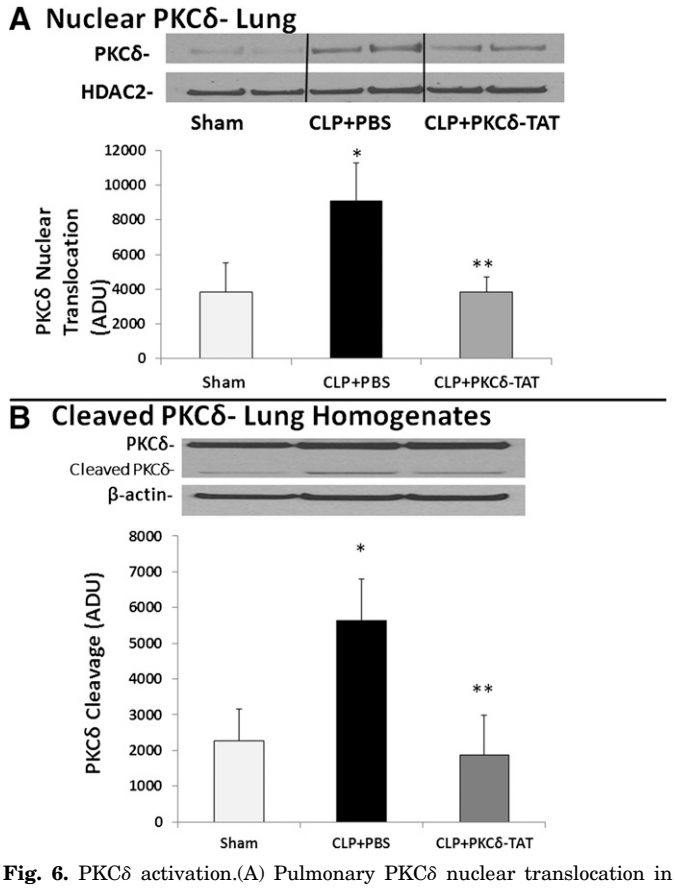

Fig. 6. PKCδ activation.(A) Pulmonary PKCδ nuclear translocation in sepsis. Targeted delivery of PKCδ-TAT peptide inhibits sepsis-induced nuclear translocation of PKCδ in the lung. Lung tissue was harvested at 24 hours postsurgery of sham-operated (Sham) animals (received 400 μl of PBS delivered IT) and CLP-operated animals that received 200 μg/kg PKCδ-TAT in 400 μl IT (CLP + PKCδ-TAT) or a similar volume of PBS vehicle only (CLP + PBS) immediately following surgery. Nuclear extracts were prepared from lung tissue homogenates, as described in *Materials and Methods*. Results are expressed as the mean ± S.E.M. (n = 7–8) in arbitrary densitometry units (ADU). *$P < 0.05$, sham versus CLP + PBS; **$P < 0.05$, CLP + PBS versus CLP + PKCδ-TAT. Representative Western blot of PKCδ in nuclear extracts and HDAC-2 as a marker for nuclear fractions.(B) Sepsis induced pulmonary proteolytic cleavage of PKCδ. Targeted delivery of PKCδ-TAT peptide inhibits sepsis-induced proteolytic cleavage of PKCδ in the lung. Lung tissue was harvested at 24 hours postsurgery of sham-operated (Sham) animals (received 400 μl of PBS delivered IT) and CLP-operated animals that received 200 μg/kg PKCδ-TAT in 400 μl IT (CLP + PKCδ-TAT) or a similar volume of PBS vehicle only (CLP + PBS) immediately following surgery. Lysates were prepared from lung tissue, as described in *Materials and Methods*, and full-length and cleaved PKCδ were identified by Western blotting. Results are expressed as the mean ± S.E.M. (n = 5–6) in arbitrary densitometry units. *$P < 0.05$, sham versus CLP + PBS; **$P < 0.05$, CLP + PBS versus CLP + PKCδ-TAT. Representative Western blot of total and cleaved (catalytic domain) PKCδ. β-Actin was used as a marker for equal protein loading.

CLP-operated animals that received TMR-PKCδ-TAT at 4, 8, and 24 hours postsurgery. There were no significant differences in the peripheral distribution of TMR-PKCδ-TAT in sham surgery animals at 4, 8, and 24 hours postsurgery (Fig. 9, A, E, and I) compared with unoperated controls (Fig. 3A). At these time points, sham-operated animals had similar lung architectures with minimal evidence of inflammation (Fig. 9, B, F, and J). Spatial lung distribution of TMR-PKCδ-TAT delivered 4 hours post-CLP was similar to sham-operated animals (Fig. 9C), whereas histopathology at 4 hours post-CLP demonstrates alveolar wall edema (thickening) but little evidence of inflammatory infiltrate (Fig. 9D).

By contrast, when the peptide was administered 8 hours post-CLP, a marked alteration in peripheral lung distribution (Fig. 9G) was observed with a lack of uniform distribution in alveolar wall cells of the distal lung parenchyma (Fig. 9G, inset) compared with sham-operated animals (Fig. 9E, inset). Histopathology at 8 hours post-CLP revealed appreciable cellular infiltrate, the filling of some alveoli, and significant loss of alveolar architecture (Fig. 9H). Spatial lung distribution of TMR-PKCδ-TAT was reduced by 75% in CLP-operated versus sham-operated animals that received peptide IT at 8 hours postsurgery (Fig. 9M; $P < 0.001$). At 24 hours post-CLP surgery, minimal peptide was observed in the lung parenchyma beyond large airways (Fig. 9K, arrows). Histopathology at 24 hours revealed destruction of alveolar wall architecture and dense inflammatory infiltrate (Fig. 9L). Spatial distribution of TMR-PKCδ-TAT was reduced by 90% in CLP-operated versus sham-operated animals that received peptide IT at 24-hours postsurgery (Fig. 9M; $P < 0.001$). These

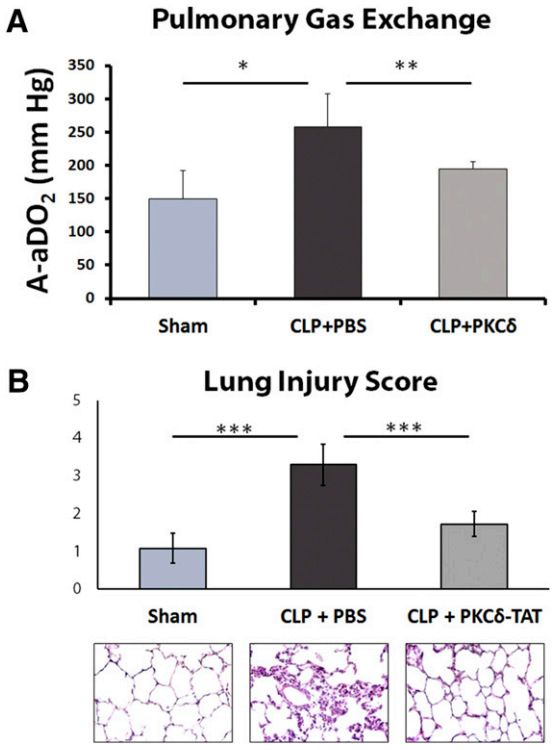

Fig. 7. Alterations in gas exchange during sepsis-induced indirect lung injury: protective effects of PKCδ-TAT. (A) Intratracheal delivery of PKCδ-TAT peptide attenuated sepsis-induced increase in intrapulmonary shunt. The A-aDO_2 gradient was measured 24 hours postsurgery in sham-operated (Sham) animals (received 400 μl of PBS delivered IT) and CLP-operated animals that received 200 μg/kg PKCδ-TAT in 400 μl IT (CLP + PKCδ-TAT) or a similar volume of PBS vehicle only (CLP + PBS) immediately following surgery. Results are expressed as the mean ± S.E.M. $^*P < 0.05$, sham versus CLP + PBS; $^{**}P < 0.05$, CLP + PBS versus CLP + PKCδ-TAT. (B) Intratracheal delivery of PKCδ-TAT attenuated histologic changes associated with CLP-induced indirect lung injury. Lung tissue was harvested at 24 hours postsurgery from animals in the sham, CLP + PBS, and CLP + PKCδ-TAT groups as described in (A). Lung injury was scored based on congestion, edema, leukocyte infiltration, and alveolar wall thickness, as described in *Materials and Methods*. H&E staining of representative lung tissues from each experimental group (400× magnification). Results are expressed as means ± S.E.M. (n = 9 rats/group). $^{***}P < 0.001$ for bracketed comparisons.

results indicate that progression of sepsis pathology significantly alters the spatial distribution of TMR-PKCδ-TAT with little peptide reaching the peripheral lung.

Effect of Delayed Administration of the PKCδ-TAT Inhibitor on Anti-inflammatory Activity in Sepsis. To investigate whether observed preservation of peptide pulmonary spatial distribution during the early time course of sepsis progression (0–4 hours post-CLP) facilitates conservation of an anti-inflammatory effect, the effect of delayed delivery of PKCδ-TAT (0, 4, and 8 hours post-CLP) on sepsis-induced increases in MPO activity was determined 24 hours post-CLP. When the peptide was administered at 0 or 4 hours post-CLP surgery, lung MPO activity levels (at 24 hours post-CLP) were significantly reduced compared with CLP-operated animals that received PBS vehicle (Fig. 10; $P < 0.01$ for 0 hours, $P < 0.05$ for 4 hours). By contrast, when the peptide was administered at 8 hours post-CLP surgery, there was a loss of PKCδ-TAT efficacy, and there were no significant differences in lung MPO levels compared with animals that received PBS vehicle.

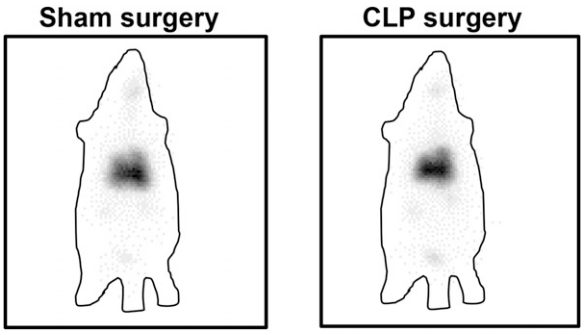

Fig. 8. Comparison of global ^{99m}Tc-PKCδ-TAT biodistribution 30 minutes following IT delivery of 500 μg/kg in 400 μl at 24 hours after sham surgery and CLP surgery. Gamma camera images. ^{99m}Tc signal is seen as black in panels. Approximate outlines of the rat bodies are shown as a lined perimeter.

Discussion

Anti-inflammatory protection of the lung during a systemic inflammatory response may improve the clinical management of indirect lung injury, such as that driven by sepsis-induced acute lung inflammation. Previously, we demonstrated that selectively inhibiting pulmonary PKCδ with a PKCδ-TAT inhibitory peptide decreased lung inflammation and prevented loss of alveolar architecture elicited by the systemic inflammatory response in an experimental model of polymicrobial abdominal sepsis (cecal ligation and puncture) (Kilpatrick et al., 2011; Mondrinos et al., 2014). The necessity of TAT conjugation for delivery of this PKCδ inhibitory peptide and other peptide cargos to tissues in vivo has been reported (Begley et al., 2004), but little is known regarding patterns of biodistribution following IT delivery of this or similar peptides. In the current study, we demonstrate that IT delivery dramatically enhances lung uptake and retention of this PKCδ-TAT peptide compared with systemic i.v. delivery with the same dose parameters (Fig. 1) and facilitates highly selective dosing of the lung (>65% ID) relative to distant organs (<5% ID in organs such as liver and kidney) (Fig. 1; Table 1). By contrast, i.v. delivery of the PKCδ-TAT inhibitory peptide resulted in diffuse uptake throughout the body, in line with previous studies that demonstrated nonspecific uptake into multiple organs, including heart, lung, and liver, when this peptide is delivered i.p. (Begley et al., 2004; Ramnath et al., 2010).

IT peptide delivery achieved reproducible spatial distribution throughout the major lung lobes (Table 2) and delivery to the peripheral lung parenchyma with peptide uptake in relevant cell types, including macrophages, endothelial cells, and type I alveolar epithelial cells (Fig. 3). Peptide delivery to the endothelium is critical, as the pulmonary endothelia are the first cells in the lung to encounter systemic proinflammatory mediators, pathogen-associated molecular patterns (PAMPS) and circulating pathogens, making them the frontline inflammatory responders during the early stages of indirect pulmonary injury. Furthermore, endothelial cell inflammation regulates neutrophil recruitment, i.e., chemokine and adhesion molecule expression, and increased permeability leading to pulmonary edema (Orfanos et al., 2004; Mondrinos et al., 2014).

PKCδ is regulated by tyrosine phosphorylation patterns on multiple sites which determine activation, localization, and substrate specificity (Steinberg, 2004, 2008; Qvit and Mochly-Rosen, 2014). We found that indirect lung injury resulting

TABLE 4
Effect of sepsis on ^{99m}Tc-PKCδ-TAT organ biodistribution
Data are the similar relative ^{99m}Tc-PKCδ-TAT organ biodistribution trends for IT delivery in normal (unoperated), sham-operated, and CLP-operated (24 hours postsurgery) animals. Organ-to-lung ratio = %ID organ/%ID lung.

Organ	Organ-to-Lung Ratio		
	Normal	24 Hours Postsham	24 Hours Post-CLP
Lung	1	1	1
Blood	0.07	0.04	0.06
Liver	0.03	0.02	0.02
Kidney	0.02	0.03	0.03

from CLP induced robust phosphorylation of PKCδ at tyrosine 311 throughout the distal lung (Fig. 4), consistent with reports of tyrosine 311 as a critical PKCδ phosphorylation site in the context of vascular inflammation (Wong et al., 2011), oxidative stress–induced apoptosis in dopaminergic neurons (Saminathan et al., 2011), and CD11b-mediated signaling in monocytes (Xue et al., 2010). Sepsis also induced widespread PKCδ tyrosine 155 phosphorylation in lung tissue (Fig. 5). In support of the hypothesis that endothelial cells are a critical target for treating indirect lung injury, endothelial cells were the primary cell type exhibiting tyrosine 155 phosphorylation as evidenced by immunohistochemical colocalization (Fig. 5). IT delivery of PKCδ-TAT significantly reduced phosphorylation of PKCδ at both tyrosine 311 and tyrosine 155 to levels comparable with sham-operated controls (Figs. 4 and 5), demonstrating that this inhibitory peptide inhibits PKCδ phosphorylation at multiple sites known to be required for proinflammatory activation.

Phosphorylation of PKCδ at tyrosine 155 and tyrosine 311 has been associated with nuclear translocation and enzyme cleavage in other cell systems (Humphries et al., 2008; Pabla et al., 2011; Zhao et al., 2012). CLP surgery induced PKCδ nuclear translocation and enzyme cleavage in the lungs of septic animals (Fig. 6). We found that IT delivery of the PKCδ-TAT peptide inhibitor attenuates sepsis-induced nuclear translocation and PKCδ cleavage in lung tissue homogenates (Fig. 6), suggesting that beneficial effects of the peptide are related to biochemical inhibition of this PKCδ activation mechanism. Nuclear translocation of PKCδ is critical for the initiation of cytotoxic or proapoptotic signaling (Humphries et al., 2008; Pabla et al., 2011), and inhibition of PKCδ nuclear translocation was reported to be cytoprotective following ischemia-reperfusion (Kostyak et al., 2006), focal cerebral ischemia (Shimohata et al., 2007), and radiation damage (Wie et al., 2014). Nuclear translocation is required for cleavage of PKCδ, which may increase PKCδ activity by removal of the regulatory domain (Okhrimenko et al., 2005). Cleavage of PKCδ has been reported following vascular injury (Yamanouchi et al., 2010), stroke (Shimohata et al., 2007), and cisplatin nephrotoxicity (Humphries et al., 2008; Pabla et al., 2011). Thus, the results of these studies are the first to demonstrate that indirect lung injury in an experimental model of sepsis induces pulmonary PKCδ tyrosine

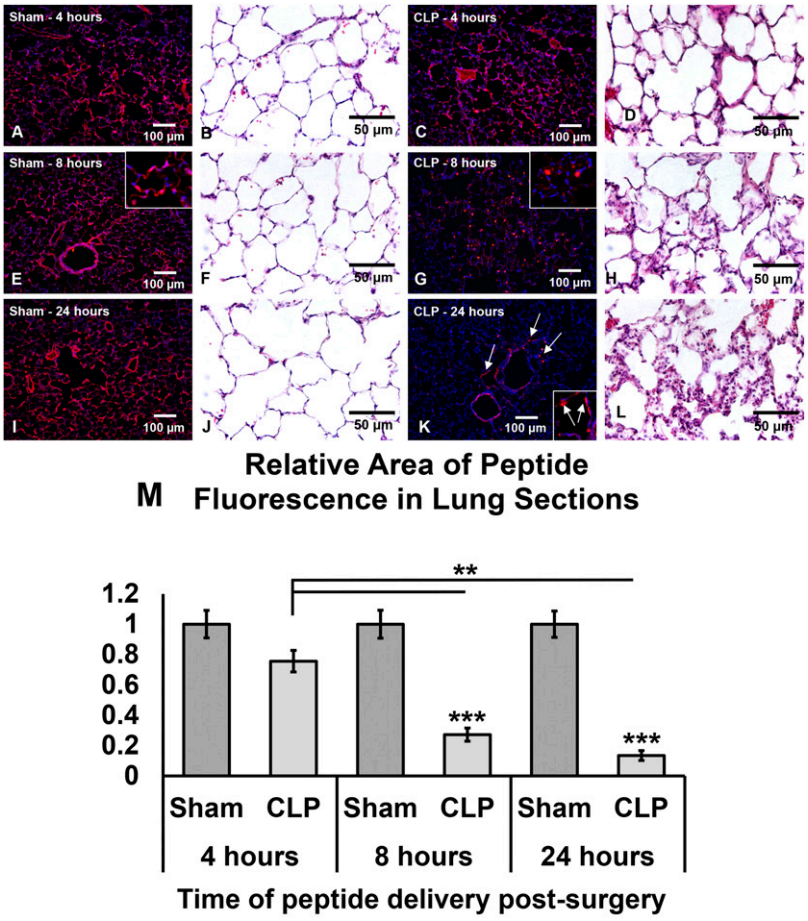

Fig. 9. Impact of sham and CLP surgery on spatial distribution of TMR-PKCδ-TAT when delivered at 4, 8, or 24 hours postsurgery. Visualization of TMR-PKCδ-TAT (red/orange fluorescence) localization in lung tissue sections. Tissue samples were harvested 30 minutes following IT delivery of TMR-PKCδ-TAT in 400 μl. Scale bars = 100 μm, original magnification = 100× for all fluorescent micrographs; scale bars = 50 μm, original magnification = 400× for all bright field micrographs. (A) TMR-PKCδ-TAT localization 4 hours postsham. (B) H&E staining 4 hours postsham. (C) TMR-PKCδ-TAT localization 4 hours post-CLP. (D) H&E staining 4 hours post-CLP. (E) TMR-PKCδ-TAT localization 8 hours postsham. (F) H&E staining 8 hours postsham. (G) TMR-PKCδ-TAT localization 8 hours post-CLP. (H) H&E staining 8 hours post-CLP. (I) TMR-PKCδ-TAT localization 24 hours postsham. (J) H&E staining 24 hours postsham. (K) TMR-PKCδ-TAT localization 24 hours post-CLP. (L) H&E staining 24 hours post-CLP. (M) Quantification of normalized TMR-positive pixel area in conditions shown in panels (A)–(F). Sham values were set equal to 1. Data were expressed as means ± S.E.M. prior to normalization (n = 4 rats/group, at least 80 fields analyzed/group); $^{**}P < 0.01$; $^{***}P < 0.001$.

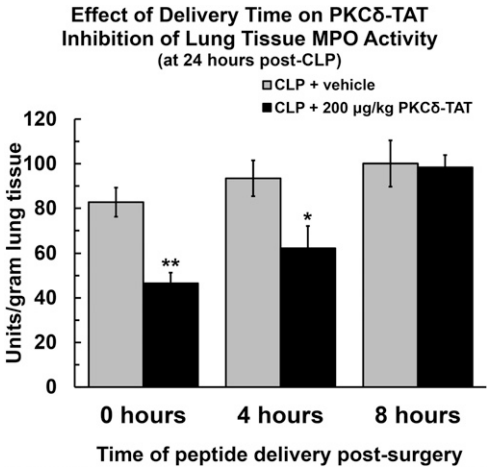

Fig. 10. MPO activity 24 hours post-CLP surgery is shown for CLP-operated rats that received PBS vehicle (400 μl) IT (gray bars) and CLP-operated rats that received 200 μg/kg in 400 μl IT (black bars) at 0 hours (immediately following surgery), 4 hours post-CLP, and 8 hours post-CLP. Data are expressed as means ± S.E.M. (n = at least 4 rats/group); *$P <$ 0.05; **$P < 0.01$. Statistical significance is indicated for comparison with CLP + vehicle at the same time point.

phosphorylation, nuclear translocation, and enzyme cleavage, all of which were significantly attenuated by IT delivery of the PKCδ-TAT peptide.

Connecting effective spatial distribution of the PKCδ-TAT inhibitory peptide and biochemical inhibition of PKCδ activity in the lung with anti-inflammatory efficacy, we demonstrate reduction of MPO activity levels in lung tissue (Table 3), consistent with our previous immunohistochemical studies demonstrating attenuation of adhesion molecule expression in the pulmonary endothelium and reduced influx of neutrophils to the lung in this sepsis model (Kilpatrick et al., 2011; Mondrinos et al., 2014). The current study builds upon cumulative evidence of anti-inflammatory efficacy to demonstrate for the first time that attenuating PKCδ activation, specifically via IT delivery of the PKCδ-TAT inhibitory peptide in this case, preserves pulmonary gas exchange function compromised by sepsis-induced indirect lung injury (Fig. 7). Significant reduction of sepsis-induced increases in A-aDO_2 would conventionally be associated with reduction of intrapulmonary shunt, and is consistent with our previous data demonstrating reduction of pulmonary edema (Kilpatrick et al., 2011). Furthermore, IT administration of the PKCδ inhibitor protected the lung from sepsis-induced pulmonary histopathological changes (Fig. 7). The histopathological profiles are consistent with preserved parenchymal and alveolar-capillary interface. Taken together, these findings provide preclinical evidence that inhibition of pulmonary PKCδ activity may be of therapeutic benefit in the setting of systemic inflammation.

An important question in critical care is how the progression of conditions such as sepsis influences organ-specific biodistribution and, consequently, the efficacy of administered therapeutics. There is a lag time between initiation of indirect pulmonary injury and lung neutrophil influx that causes tissue injury (Bhatia and Moochhala, 2004). This lag period, dependent on type and severity of injury, may offer a therapeutic window in which treatment could be initiated to stop the progression of indirect lung injury. In the present study, we show experimental evidence of a therapeutic window by demonstrating that reduction of lung MPO activity with IT delivery of PKCδ-TAT at 4 hours post-CLP is similar to the level of lung MPO reduction observed with delivery at the time of sepsis induction (Fig. 10). The CLP model of sepsis used in this study is highly lethal, with a mortality of approximately 70% at 48 hours and animals becoming severely ill within 8 hours of the CLP procedure (Weiss et al., 2000, 2002). Preservation of efficacy with delivery at 4 hours after sepsis induction correlated with a preservation of lung architecture and spatial peptide distribution comparable to sham-operated controls (Fig. 9).

Although the degree to which anti-inflammatory efficacy is dependent on peptide spatial distribution cannot be elucidated based on the current data, our observations are relevant to time dependency of delivery in this disease model. The inability of PKCδ-TAT to reduce CLP-induced lung MPO activity levels when delivered at 8 hours post-CLP (Fig. 10) corresponded to a disruption of lung architecture and reduced PKCδ-TAT peptide spatial distribution in the peripheral lung (Fig. 9). Sepsis-induced increases in lung permeability and the development of pulmonary edema may interfere with transport processes that affect peptide distribution and cellular uptake in the lung. In addition, the presence of macrophage and neutrophil-derived proteases may promote cleavage and peptide degradation (Brehm et al., 2014), which is further exacerbated by possible disruption of the antiprotease balance following CLP surgery (Cryan, 2005). These findings are in agreement with other studies which demonstrated a clear relationship between pathologic changes in tissue and organ architecture associated with pathogen-mediated immune responses and impaired therapeutic biodistribution (Barbosa et al., 2009).

In summary, utilizing a combination of radiolabeling and fluorescent-tagging approaches to analyze organ and cellular biodistribution of a PKCδ-TAT peptide inhibitor, we demonstrate highly selective lung targeting and relative uniformity of peptide spatial distribution in the lung following IT delivery. Sepsis induced significant pulmonary activation of PKCδ as assessed by tyrosine 155 and 311 phosphorylation, nuclear PKCδ translocation, and enzyme cleavage, which was attenuated by the PKCδ-TAT peptide, indicating functional efficacy of the peptide inhibitor delivered by the IT route. Functional studies demonstrate that the inhibitor was lung-protective and reduced sepsis-induced neutrophil influx (MPO) into the lung and preserved lung function and gas exchange. Although our study suggests that targeted inhibition of PKCδ may offer an attractive therapeutic option for the treatment of sepsis-induced acute lung injury, further studies are required to determine 1) the protective effects of this inhibitor at longer time points, 2) the effect of multiple dosing over the course of development of the sepsis pathology, and 3) whether such a treatment program with this inhibitor offers a survival benefit.

Authorship Contributions

Participated in research design: Mondrinos, Knight, Wolfson, Kilpatrick.

Conducted experiments: Mondrinos, Kennedy, Wu, Kauffman, Baker.

Performed data analysis: Mondrinos, Knight, Wolfson, Kilpatrick.

Wrote or contributed to the writing of the manuscript: Mondrinos, Knight, Wolfson, Kilpatrick.

References

Abraham E (2003) Neutrophils and acute lung injury. *Crit Care Med* **31**(4, Suppl) S195–S199.

Bai J, Tang L, Lomas-Neira J, Chen Y, McLeish KR, Uriarte SM, Chung CS, and Ayala A (2015) TAT-SNAP-23 treatment inhibits the priming of neutrophil functions contributing to shock and/or sepsis-induced extra-pulmonary acute lung injury. *Innate Immun* **21**:42–54.

Barbosa VS, Holanda CM, Câmara AC, Silva RP, Oliveira DP, Moreira JA, and Medeiros AC (2009) Trypanosoma cruzi: biodistribution of technetium-99m pertechnetate in infected rats. *Exp Parasitol* **123**:309–312.

Bates E, Bode C, Costa M, Gibson CM, Granger C, Green C, Grimes K, Harrington R, Huber K, and Kleiman N, et al.; Direct Inhibition of delta-Protein Kinase C Enzyme to Limit Total Infarct Size in Acute Myocardial Infarction (DELTA MI) Investigators (2008) Intracoronary KAI-9803 as an adjunct to primary percutaneous coronary intervention for acute ST-segment elevation myocardial infarction. *Circulation* **117**:886–896.

Begley R, Liron T, Baryza J, and Mochly-Rosen D (2004) Biodistribution of intracellularly acting peptides conjugated reversibly to Tat. *Biochem Biophys Res Commun* **318**:949–954.

Bhatia M and Moochhala S (2004) Role of inflammatory mediators in the pathophysiology of acute respiratory distress syndrome. *J Pathol* **202**:145–156.

Brehm A, Geraghty P, Campos M, Garcia-Arcos I, Dabo AJ, Gaffney A, Eden E, Jiang XC, D'Armiento J, and Foronjy R (2014) Cathepsin G degradation of phospholipid transfer protein (PLTP) augments pulmonary inflammation. *FASEB J* **28**: 2318–2331.

Cai S-R, Xu G, Becker-Hapak M, Ma M, Dowdy SF, and McLeod HL (2006) The kinetics and tissue distribution of protein transduction in mice. *Eur J Pharm Sci* **27**:311–319.

Chen L, Hahn H, Wu G, Chen CH, Liron T, Schechtman D, Cavallaro G, Banci L, Guo Y, and Bolli R, et al. (2001) Opposing cardioprotective actions and parallel hypertrophic effects of delta PKC and epsilon PKC. *Proc Natl Acad Sci USA* **98**: 11114–11119.

Cheong SH, Yang YI, Seo JY, Jun DH, Ko MJ, Cho KR, Lee SE, Kim YH, Lim SH, and Lee JH, et al. (2010) Unilateral administration of a drug into the lung of a small animal. *Korean J Anesthesiol* **58**:283–289.

Chichger H, Grinnell KL, Casserly B, Chung CS, Braza J, Lomas-Neira J, Ayala A, Rounds S, Klinger JR, and Harrington EO (2012) Genetic disruption of protein kinase Cδ reduces endotoxin-induced lung injury. *Am J Physiol Lung Cell Mol Physiol* **303**:L880–L888.

Chou WH, Choi DS, Zhang H, Mu D, McMahon T, Kharazia VN, Lowell CA, Ferriero DM, and Messing RO (2004) Neutrophil protein kinase Cdelta as a mediator of stroke-reperfusion injury. *J Clin Invest* **114**:49–56.

Churchill E, Budas G, Vallentin A, Koyanagi T, and Mochly-Rosen D (2008) PKC isozymes in chronic cardiac disease: possible therapeutic targets? *Annu Rev Pharmacol Toxicol* **48**:569–599.

Cohen P (2009) Targeting protein kinases for the development of anti-inflammatory drugs. *Curr Opin Cell Biol* **21**:317–324.

Cryan S-A (2005) Carrier-based strategies for targeting protein and peptide drugs to the lungs. *AAPS J* **7**:E20–E41.

Deutschman CS and Tracey KJ (2014) Sepsis: current dogma and new perspectives. *Immunity* **40**:463–475.

DeVries-Seimon TA, Ohm AM, Humphries MJ, and Reyland ME (2007) Induction of apoptosis is driven by nuclear retention of protein kinase C δ. *J Biol Chem* **282**: 22307–22314.

Driscoll KE, Costa DL, Hatch G, Henderson R, Oberdorster G, Salem H, and Schlesinger RB (2000) Intratracheal instillation as an exposure technique for the evaluation of respiratory tract toxicity: uses and limitations. *Toxicol Sci* **55**: 24–35.

Fehrenbach A, Ochs M, Wittwer T, Cornelius J, Fehrenbach H, Wahlers T, and Richter J (1999) Stereological estimation of the volume weighted mean volumes of alveoli and acinar pathways in the rat lung to characterise alterations after ischaemia/reperfusion. *J Anat* **194**:127–135.

Gaestel M, Kotlyarov A, and Kracht M (2009) Targeting innate immunity protein kinase signalling in inflammation. *Nat Rev Drug Discov* **8**:480–499.

Ghayur T, Hugunin M, Talanian RV, Ratnofsky S, Quinlan C, Emoto Y, Pandey P, Datta R, Huang Y, and Kharbanda S, et al. (1996) Proteolytic activation of protein kinase C delta by an ICE/CED 3-like protease induces characteristics of apoptosis. *J Exp Med* **184**:2399–2404.

Humphries MJ, Ohm AM, Schaack J, Adwan TS, and Reyland ME (2008) Tyrosine phosphorylation regulates nuclear translocation of PKCdelta. delta *Oncogene* **27**: 3045–3053.

Iskander KN, Osuchowski MF, Stearns-Kurosawa DJ, Kurosawa S, Stepien D, Valentine C, and Remick DG (2013) Sepsis: multiple abnormalities, heterogeneous responses, and evolving understanding. *Physiol Rev* **93**:1247–1288.

Kilpatrick LE, Standage SW, Li H, Raj NR, Korchak HM, Wolfson MR, and Deutschman CS (2011) Protection against sepsis-induced lung injury by selective inhibition of protein kinase C-δ (δ-PKC). *J Leukoc Biol* **89**:3–10.

Kilpatrick LE, Sun S, Li H, Vary TC, and Korchak HM (2010) Regulation of TNF-induced oxygen radical production in human neutrophils: role of delta-PKC. *J Leukoc Biol* **87**:153–164.

Kleemann E, Neu M, Jekel N, Fink L, Schmehl T, Gessler T, Seeger W, and Kissel T (2005) Nano-carriers for DNA delivery to the lung based upon a TAT-derived peptide covalently coupled to PEG-PEI. *J Control Release* **109**:299–316.

Knight LC, Romano JE, Bright LT, Agelan A, Kantor S, and Maurer AH (2007) Platelet binding and biodistribution of [99mTc]rBitistatin in animal species and humans. *Nucl Med Biol* **34**:855–863.

Kostyak JC, Hunter JC, and Korzick DH (2006) Acute PKCdelta inhibition limits ischaemia-reperfusion injury in the aged rat heart: role of GSK-3β. *Cardiovasc Res* **70**:325–334.

Kronfeld I, Kazimirsky G, Lorenzo PS, Garfield SH, Blumberg PM, and Brodie C (2000) Phosphorylation of protein kinase Cdelta on distinct tyrosine residues regulates specific cellular functions. *J Biol Chem* **275**:35491–35498.

MacIntyre NR (2001) Intratracheal catheters as drug delivery systems. *Respir Care* **46**:193–197.

Matthay MA and Zemans RL (2011) The acute respiratory distress syndrome: pathogenesis and treatment. *Annu Rev Pathol* **6**:147–163.

Mondrinos MJ, Kennedy PA, Lyons M, Deutschman CS, and Kilpatrick LE (2013) Protein kinase C and acute respiratory distress syndrome. *Shock* **39**:467–479.

Mondrinos MJ, Zhang T, Sun S, Kennedy PA, King DJ, Wolfson MR, Knight LC, Scalia R, and Kilpatrick LE (2014) Pulmonary endothelial protein kinase C-delta (PKCδ) regulates neutrophil migration in acute lung inflammation. *Am J Pathol* **184**:200–213.

Moschos SA, Jones SW, Perry MM, Williams AE, Erjefalt JS, Turner JJ, Barnes PJ, Sproat BS, Gait MJ, and Lindsay MA (2007) Lung delivery studies using siRNA conjugated to TAT(48-60) and penetratin reveal peptide induced reduction in gene expression and induction of innate immunity. *Bioconjug Chem* **18**:1450–1459.

Müller S and Knapp S (2010) Targeting kinases for the treatment of inflammatory diseases. *Expert Opin Drug Discov* **5**:867–881.

Nguyen J, Xie X, Neu M, Dumitrascu R, Reul R, Sitterberg J, Bakowsky U, Schermuly R, Fink L, and Schmehl T, et al. (2008) Effects of cell-penetrating peptides and pegylation on transfection efficiency of polyethylenimine in mouse lungs. *J Gene Med* **10**:1236–1246.

Okhrimenko H, Lu W, Xiang C, Ju D, Blumberg PM, Gomel R, Kazimirsky G, and Brodie C (2005) Roles of tyrosine phosphorylation and cleavage of protein kinase Cdelta in its protective effect against tumor necrosis factor-related apoptosis inducing ligand-induced apoptosis. *J Biol Chem* **280**:23643–23652.

Orfanos SE, Mavrommati I, Korovesi I, and Roussos C (2004) Pulmonary endothelium in acute lung injury: from basic science to the critically ill. *Intensive Care Med* **30**:1702–1714.

Pabla N, Dong G, Jiang M, Huang S, Kumar MV, Messing RO, and Dong Z (2011) Inhibition of PKCδ reduces cisplatin-induced nephrotoxicity without blocking chemotherapeutic efficacy in mouse models of cancer. *J Clin Invest* **121**: 2709–2722.

Page K, Li J, Zhou L, Iasvovskaia S, Corbit KC, Soh JW, Weinstein IB, Brasier AR, Lin A, and Hershenson MB (2003) Regulation of airway epithelial cell NF-kappa B-dependent gene expression by protein kinase C delta. *J Immunol* **170**:5681–5689.

Perl M, Lomas-Neira J, Venet F, Chung C-S, and Ayala A (2011) Pathogenesis of indirect (secondary) acute lung injury. *Expert Rev Respir Med* **5**:115–126.

Qi X, Inagaki K, Sobel RA, and Mochly-Rosen D (2008) Sustained pharmacological inhibition of deltaPKC protects against hypertensive encephalopathy through prevention of blood-brain barrier breakdown in rats. *J Clin Invest* **118**:173–182.

Qin Y, Zhang Q, Chen H, Yuan W, Kuai R, Xie F, Zhang L, Wang X, Zhang Z, and Liu J, et al. (2012) Comparison of four different peptides to enhance accumulation of liposomes into the brain. *J Drug Target* **20**:235–245.

Qvit N and Mochly-Rosen D (2014) The many hats of protein kinase Cδ: one enzyme with many functions. *Biochem Soc Trans* **42**:1529–1533.

Ramnath RD, Sun J, and Bhatia M (2010) PKC δ mediates pro-inflammatory responses in a mouse model of caerulein-induced acute pancreatitis. *J Mol Med (Berl)* **88**:1055–1063.

Ranieri VM, Rubenfeld GD, Thompson BT, Ferguson ND, Caldwell E, Fan E, Camporota L, and Slutsky AS; ARDS Definition Task Force (2012) Acute respiratory distress syndrome: the Berlin Definition. *JAMA* **307**:2526–2533.

Reutershan J and Ley K (2004) Bench-to-bedside review: acute respiratory distress syndrome - how neutrophils migrate into the lung. *Crit Care* **8**:453–461.

Rittirsch D, Huber-Lang MS, Flierl MA, and Ward PA (2009) Immunodesign of experimental sepsis by cecal ligation and puncture. *Nat Protoc* **4**:31–36.

Rose L, Kenny L, Tait G, and Mehta S (2014) Ventilator settings and monitoring parameter targets for initiation of continuous mandatory ventilation: a questionnaire study. *J Crit Care* **29**:123–127.

Salter JW, Krieglstein CF, Issekutz AC, and Granger DN (2001) Platelets modulate ischemia/reperfusion-induced leukocyte recruitment in the mesenteric circulation. *Am J Physiol Gastrointest Liver Physiol* **281**:G1432–G1439.

Saminathan H, Asaithambi A, Anantharam V, Kanthasamy AG, and Kanthasamy A (2011) Environmental neurotoxic pesticide dieldrin activates a non receptor tyrosine kinase to promote PKCδ-mediated dopaminergic apoptosis in a dopaminergic neuronal cell model. *Neurotoxicology* **32**:567–577.

Schwarze SR, Ho A, Vocero-Akbani A, and Dowdy SF (1999) In vivo protein transduction: delivery of a biologically active protein into the mouse. *Science* **285**: 1569–1572.

Shimohata T, Zhao H, Sung JH, Sun G, Mochly-Rosen D, and Steinberg GK (2007) Suppression of deltaPKC activation after focal cerebral ischemia contributes to the protective effect of hypothermia. *J Cereb Blood Flow Metab* **27**:1463–1475.

Steinberg SF (2004) Distinctive activation mechanisms and functions for protein kinase Cdelta. *Biochem J* **384**:449–459.

Steinberg SF (2008) Structural basis of protein kinase C isoform function. *Physiol Rev* **88**:1341–1378.

Stevenson EK, Rubenstein AR, Radin GT, Wiener RS, and Walkey AJ (2014) Two decades of mortality trends among patients with severe sepsis: a comparative meta-analysis*. *Crit Care Med* **42**:625–631.

Sutherasan Y, Vargas M, and Pelosi P (2014) Protective mechanical ventilation in the non-injured lung: review and meta-analysis. *Crit Care* **18**:211.

Torchilin VP, Rammohan R, Weissig V, and Levchenko TS (2001) TAT peptide on the surface of liposomes affords their efficient intracellular delivery even at low temperature and in the presence of metabolic inhibitors. *Proc Natl Acad Sci USA* **98**: 8786–8791.

Villar J, Sulemanji D, and Kacmarek RM (2014) The acute respiratory distress syndrome: incidence and mortality, has it changed? *Curr Opin Crit Care* **20**:3–9.

Vivès E, Richard JP, Rispal C, and Lebleu B (2003) TAT peptide internalization: seeking the mechanism of entry. *Curr Protein Pept Sci* **4**:125–132.

Weiss YG, Bouwman A, Gehan B, Schears G, Raj N, and Deutschman CS (2000) Cecal ligation and double puncture impairs heat shock protein 70 (HSP-70) expression in the lungs of rats. *Shock* **13**:19–23.
Weiss YG, Maloyan A, Tazelaar J, Raj N, and Deutschman CS (2002) Adenoviral transfer of HSP-70 into pulmonary epithelium ameliorates experimental acute respiratory distress syndrome. *J Clin Invest* **110**:801–806.
Wie SM, Adwan TS, DeGregori J, Anderson SM, and Reyland ME (2014) Inhibiting tyrosine phosphorylation of protein kinase Cδ (PKCδ) protects the salivary gland from radiation damage. *J Biol Chem* **289**:10900–10908.
Wong SL, Lau CW, Wong WT, Xu A, Au CL, Ng CF, Ng SS, Gollasch M, Yao X, and Huang Y (2011) Pivotal role of protein kinase Cdelta in angiotensin II-induced endothelial cyclooxygenase-2 expression: a link to vascular inflammation. *Arterioscler Thromb Vasc Biol* **31**:1169–1176.
Xue ZH, Zhao CQ, Chua GL, Tan SW, Tang XY, Wong SC, and Tan SM (2010) Integrin alphaMbeta2 clustering triggers phosphorylation and activation of protein kinase C delta that regulates transcription factor Foxp1 expression in monocytes. *J Immunol* **184**:3697–3709.
Yamanouchi D, Kato K, Ryer EJ, Zhang F, and Liu B (2010) Protein kinase C delta mediates arterial injury responses through regulation of vascular smooth muscle cell apoptosis. *Cardiovasc Res* **85**:434–443.
Zhao M, Xia L, and Chen G-Q (2012) Protein kinase cδ in apoptosis: a brief overview. *Arch Immunol Ther Exp (Warsz)* **60**:361–372.

Address correspondence to: Dr. Laurie E. Kilpatrick, Center for Inflammation, Translational and Clinical Lung Research, Temple University School of Medicine, 3500 North Broad Street, Room 1153, Medical Education and Research Building, Philadelphia, PA 19140. E-mail: laurie.kilpatrick@temple.edu